Femtosecond infrared intrastromal ablation and backscattering-mode adaptive-optics multiphoton microscopy in chicken corneas

Emilio J. Gualda,[1] Javier R. Vázquez de Aldana,[2] M. Carmen Martínez-García,[3] Pablo Moreno,[2] Juan Hernández-Toro,[2] Luis Roso,[4] Pablo Artal,[1] and Juan M. Bueno[1,*]

[1]*Laboratorio de Óptica, Centro de Investigación en Óptica y Nanofísica, Universidad de Murcia, Campus de Espinardo (Edificio 34), 30100 Murcia, Spain*

[2]*Grupo de Investigación en Microprocesado de Materiales con Láser,Plaza de la Merced s/n, 37008 Salamanca, Spain*

[3]*Departamento Biología Celular, Histología y Farmacología,Facultad de Medicina, Universidad de Valladolid, Valladolid, Spain*

[4]*Centro de Láseres Pulsados Ultracortos y Ultraintensos (CLPU), Plaza de la Merced s/n, 37008 Salamanca, Spain*

**bueno@um.es*

Abstract: The performance of femtosecond (fs) laser intrastromal ablation was evaluated with backscattering-mode adaptive-optics multiphoton microscopy in *ex vivo* chicken corneas. The pulse energy of the fs source used for ablation was set to generate two different ablation patterns within the corneal stroma at a certain depth. Intrastromal patterns were imaged with a custom adaptive-optics multiphoton microscope to determine the accuracy of the procedure and verify the outcomes. This study demonstrates the potential of using fs pulses as surgical and monitoring techniques to systematically investigate intratissue ablation. Further refinement of the experimental system by combining both functions into a single fs laser system would be the basis to establish new techniques capable of monitoring corneal surgery without labeling in real-time. Since the backscattering configuration has also been optimized, future *in vivo* implementations would also be of interest in clinical environments involving corneal ablation procedures.

OCIS codes: (170.3880) Medical and biological imaging; (180.4315) Nonlinear microscopy; (170.1020) Ablation of tissue; (170.4470) Ophthalmology

References and links

1. M. M. Krasnov, "Q-switched laser goniopuncture," Arch. Ophthalmol. **92**(1), 37–41 (1974).
2. D. Aron-Rosa, J. J. Aron, M. Griesemann, and R. Thyzel, "Use of the neodymium-YAG laser to open the posterior capsule after lens implant surgery: a preliminary report," J. Am. Intraocul. Implant Soc. **6**(4), 352–354 (1980).
3. R. M. Klapper, "Q-switched neodymium:YAG laser iridotomy," Ophthalmology **91**(9), 1017–1021 (1984).
4. A. Vogel, "Nonlinear absorption: intraocular microsurgery and laser lithotripsy," Phys. Med. Biol. **42**(5), 895–912 (1997).
5. A. Vogel, A. Noack, K. Nahen, D. Theisen, R. Birngruber, D. X. Hammer, G. D. Noojin, and B. A. Rockwell, "Laser-induced breakdown in the eye at pulse durations from 80 ns to 100 fs," Proc. SPIE **3255**, 43–49 (1998).
6. R. R. Krueger, S. L. Trokel, and H. D. Schubert, "Interaction of ultraviolet laser light with the cornea," Invest. Ophthalmol. Vis. Sci. **26**(11), 1455–1464 (1985).
7. I. G. Pallikaris, M. E. Papatzanaki, E. Z. Stathi, O. Frenschock, and A. Georgiadis, "Laser in situ keratomileusis," Lasers Surg. Med. **10**(5), 463–468 (1990).
8. I. G. Pallikaris and D. S. Siganos, "Excimer laser in situ keratomileusis and photorefractive keratectomy for correction of high myopia," J. Refract. Corneal Surg. **10**(5), 498–510 (1994).
9. A. Vogel, J. Noack, G. Hüttman, and G. Paltauf, "Mechanism of femtosecond laser nanosurgery of cells and tissues," Appl. Phys. B **81**(8), 1015–1047 (2005).
10. H. Lubatschowski, G. Maatz, A. Heisterkamp, U. Hetzel, W. Drommer, H. Welling, and W. Ertmer, "Application of ultrashort laser pulses for intrastromal refractive surgery," Graefes Arch. Clin. Exp. Ophthalmol. **238**(1), 33–39 (2000).
11. W. Denk, J. H. Strickler, and W. W. Webb, "Two-photon laser scanning fluorescence microscopy," Science **248**(4951), 73–76 (1990).

#150262 - $15.00 USD Received 1 Jul 2011; revised 27 Sep 2011; accepted 27 Sep 2011; published 3 Oct 2011

12. P. J. Campagnola, H. A. Clark, W. A. Mohler, A. Lewis, and L. M. Loew, "Second-harmonic imaging microscopy of living cells," J. Biomed. Opt. **6**(3), 277–286 (2001).
13. L. T. Nordan, S. G. Slade, R. N. Baker, C. Suárez, T. Juhasz, and R. Kurtz, "Femtosecond laser flap creation for laser in situ keratomileusis: six-month follow-up of initial U.S. clinical series," J. Refract. Surg. **19**(1), 8–14 (2003).
14. R. M. Kurtz, C. Horvath, H. H. Liu, R. R. Krueger, and T. Juhasz, "Lamellar refractive surgery with scanned intrastromal picosecond and femtosecond laser pulses in animal eyes," J. Refract. Surg. **14**(5), 541–548 (1998).
15. D. Giguère, G. Olivié, F. Vidal, S. Toetsch, G. Girard, T. Ozaki, J.-C. Kieffer, O. Nada, and I. Brunette, "Laser ablation threshold dependence on pulse duration for fused silica and corneal tissues: experiments and modeling," J. Opt. Soc. Am. A **24**(6), 1562–1568 (2007).
16. M. Han, G. Giese, L. Zickler, H. Sun, and J. F. Bille, "Mini-invasive corneal surgery and imaging with femtosecond lasers," Opt. Express **12**(18), 4275–4281 (2004).
17. K. Koenig, O. Krauss, and I. Riemann, "Intratissue surgery with 80 MHz nanojoule femtosecond laser pulses in the near infrared," Opt. Express **10**(3), 171–176 (2002).
18. G. Olivié, D. Giguère, F. Vidal, T. Ozaki, J. C. Kieffer, O. Nada, and I. Brunette, "Wavelength dependence of femtosecond laser ablation threshold of corneal stroma," Opt. Express **16**(6), 4121–4129 (2008).
19. R. M. Kurtz, X. Liu, V. M. Elner, J. A. Squier, D. Du, and G. A. Mourou, "Photodisruption in the human cornea as a function of laser pulse width," J. Refract. Surg. **13**(7), 653–658 (1997).
20. H. Sun, M. Han, M. H. Niemz, and J. F. Bille, "Femtosecond laser corneal ablation threshold: dependence on tissue depth and laser pulse width," Lasers Surg. Med. **39**(8), 654–658 (2007).
21. H. K. Soong, S. Mian, O. Abbasi, and T. Juhasz, "Femtosecond laser-assisted posterior lamellar keratoplasty: initial studies of surgical technique in eye bank eyes," Ophthalmology **112**(1), 44–49 (2005).
22. V. Nuzzo, K. Plamann, M. Savoldelli, M. Merano, D. Donate, O. Albert, P. F. Gardeazábal Rodríguez, G. Mourou, and J. M. Legeais, "In situ monitoring of second-harmonic generation in human corneas to compensate for femtosecond laser pulse attenuation in keratoplasty," J. Biomed. Opt. **12**(6), 064032 (2007).
23. T. Ripken, U. Oberheide, M. Fromm, S. Schumacher, G. Gerten, and H. Lubatschowski, "fs-Laser induced elasticity changes to improve presbyopic lens accommodation," Graefes Arch. Clin. Exp. Ophthalmol. **246**(6), 897–906 (2008).
24. L. Ding, W. H. Knox, J. Bühren, L. J. Nagy, and K. R. Huxlin, "Intratissue refractive index shaping (IRIS) of the cornea and lens using a low-pulse-energy femtosecond laser oscillator," Invest. Ophthalmol. Vis. Sci. **49**(12), 5332–5339 (2008).
25. H. Nakamura, Y. Liu, T. E. Witt, R. J. Gordon, and D. P. Edward, "Femtosecond laser photodisruption of primate trabecular meshwork: an *ex vivo* study," Invest. Ophthalmol. Vis. Sci. **50**(3), 1198–1204 (2009).
26. U. Vossmerbaeumer and J. B. Jonas, "Structure of intracorneal femtosecond laser pulse effects in conical incision profiles," Graefes Arch. Clin. Exp. Ophthalmol. **246**(7), 1017–1020 (2008).
27. M. Han, L. Zickler, G. Giese, M. Walter, F. H. Loesel, and J. F. Bille, "Second-harmonic imaging of cornea after intrastromal femtosecond laser ablation," J. Biomed. Opt. **9**(4), 760–766 (2004).
28. B. G. Wang, I. Riemann, H. Schubert, D. Schweitzer, K. König, and K. J. Halbhuber, "Multiphoton microscopy for monitoring intratissue femtosecond laser surgery effects," Lasers Surg. Med. **39**(6), 527–533 (2007).
29. E. J. Gualda, J. M. Bueno, and P. Artal, "Wavefront optimized nonlinear microscopy of *ex vivo* human retinas," J. Biomed. Opt. **15**(2), 026007 (2010).
30. J. M. Bueno, E. J. Gualda, and P. Artal, "Adaptive optics multiphoton microscopy to study *ex vivo* ocular tissues," J. Biomed. Opt. **15**(6), 066004 (2010).
31. J. M. Bueno, A. Giakoumaki, E. J. Gualda, F. Schaeffel, and P. Artal, "Analysis of the chicken retina with an adaptive optics multiphoton microscope," Biomed. Opt. Express **2**(6), 1637–1648 (2011).
32. L. J. Nagy, L. Ding, L. Xu, W. H. Knox, and K. R. Huxlin, "Potentiation of femtosecond laser intratissue refractive index shaping (IRIS) in the living cornea with sodium fluorescein," Invest. Ophthalmol. Vis. Sci. **51**(2), 850–856 (2010).
33. L. Jay, A. Brocas, K. Singh, J. C. Kieffer, I. Brunette, and T. Ozaki, "Determination of porcine corneal layers with high spatial resolution by simultaneous second and third harmonic generation microscopy," Opt. Express **16**(21), 16284–16293 (2008).
34. S.-Y. Chen, H.-C. Yu, I.-J. Wang, and C.-K. Sun, "Infrared-based third and second harmonic generation imaging of cornea," J. Biomed. Opt. **14**(4), 044012 (2009).
35. B. G. Wang, I. Riemann, H. Schubert, K. J. Halbhuber, and K. Koenig, "In-vivo intratissue ablation by nanojoule near-infrared femtosecond laser pulses," Cell Tissue Res. **328**(3), 515–520 (2007).
36. N. Morishige, A. Kesler-Diaz, A. J. Wahlert, R. M. Kurtz, T. Juhasz, M. Sarayba, and J. V. Jester, "Corneal response to femtosecond laser photodisruption in the rabbit," Exp. Eye Res. **86**(5), 835–843 (2008).
37. M. Han, G. Giese, and J. F. Bille, "Second harmonic generation imaging of collagen fibrils in cornea and sclera," Opt. Express **13**(15), 5791–5797 (2005).
38. J. M. Bueno, E. J. Gualda, and P. Artal, "Analysis of corneal stroma organization with wavefront optimized nonlinear microscopy," Cornea **30**(6), 692–701 (2011).
39. J. M. Bueno, E. J. Gualda, A. Giakoumaki, P. Pérez-Merino, S. Marcos, and P. Artal, "Multiphoton microscopy of *ex vivo* corneas after collagen cross-linking," Invest. Ophthalmol. Vis. Sci. **52**(8), 5325–5331 (2011).
40. V. Hovhannisyan, W. Lo, C. Hu, S. J. Chen, and C. Y. Dong, "Dynamics of femtosecond laser photo-modification of collagen fibers," Opt. Express **16**(11), 7958–7968 (2008).
41. V. Hovhannisyan, A. Ghazaryan, Y. F. Chen, S. J. Chen, and C. Y. Dong, "Photophysical mechanisms of collagen modification by 80 MHz femtosecond laser," Opt. Express **18**(23), 24037–24047 (2010).

#150262 - $15.00 USD Received 1 Jul 2011; revised 27 Sep 2011; accepted 27 Sep 2011; published 3 Oct 2011

42. T. J. Wang, W. Lo, C. M. Hsueh, M. S. Hsieh, C. Y. Dong, and F. R. Hu, "*Ex vivo* multiphoton analysis of rabbit corneal wound healing following conductive keratoplasty," J. Biomed. Opt. **13**(3), 034019 (2008).
43. B.-G. Wang and K.-J. Halbhuber, "Corneal multiphoton microscopy and intratissue optical nanosurgery by nanojoule femtosecond near-infrared pulsed lasers," Ann. Anat. **188**(5), 395–409 (2006).
44. M. Hao, K. Flynn, C. Nien-Shy, B. E. Jester, M. Winkler, D. J. Brown, O. La Schiazza, J. F. Bille, and J. V. Jester, "*In vivo* non-linear optical (NLO) imaging in live rabbit eyes using the Heidelberg Two-Photon Laser Ophthalmoscope," Exp. Eye Res. **91**(2), 308–314 (2010).

1. Introduction

Photodisruption of ocular tissues with pulsed lasers was introduced by Krasnov in 1974 [1] and has been used for different ophthalmic surgery techniques during the last decades [2–5]. In particular, corneal refractive surgery by means of ultraviolet (UV) nanosecond (ns) pulses has been widely used for the correction of refractive errors [6–8]. This kind of surgery is based on the ablation of the corneal tissue through one-photon absorption of UV light.

More recently, near-infrared (NIR) femtosecond (fs) lasers have provided an additional tool for corneal surgery, since these NIR pulses can pass the corneal tissue without significant one-photon absorption. When the pulses are tightly focused inside the tissue, the intensity in the focal volume leads to nonlinear (multiphoton) phenomena. If the power density is high enough, photodisruption would take place [9,10]. However a power below a certain threshold to avoid the optical breakdown also allows the use of these sources for the so-called multiphoton microscopy, based on two different phenomena known as two-photon excitation fluorescence (TPEF) [11] and second harmonic generation (SHG) [12]. Since the absorption within the tissue is nonlinear, both multiphoton microscopy and photodisruption effects are highly localized, and the fs laser irradiation hardly affects the surrounding regions outside the focal volume.

Nowadays the main clinical application of NIR fs lasers includes corneal flap creation prior to refractive surgery [13]. However, since the first demonstration of NIR fs intrastromal refractive surgery [14] the effect of different parameters, such as the pulse energy (laser power) [10,15,16], laser repetition rate [17], wavelength [18], pulse width [19] and tissue depth [20] have been studied. Moreover the use of NIR fs lasers might also open the door to future new clinical applications such as keratoplasty (corneal transplantation surgery) [21,22], lentotomy [23], intratissue refractive index shaping [24] and trabecular meshwork surgery [25]. However, to our knowledge, there is a lack of efficient techniques to evaluate the performance of intrastromal corneal ablation procedures. Most experiments included a postmortem analysis by means of histological techniques [10,22,26]. This is a tedious operation which requires fixation, staining and slicing of very thin histological corneal sections. This may introduce undesired retraction by dehydration, leading to imaging artifacts.

Alternative analyses using non-invasive imaging techniques of the intact cornea are desirable. In particular, some authors have suggested the use of SHG signal arising from the corneal stroma as a tool for the visualization of corneal flaps [17] and isolated cavitation bubbles [20,27,28].

The objective of this work is to create and analyze ablation intrastromal patterns on chicken corneas. These will be visualized with multiphoton microscopy. This will show the feasibility of this imaging technique for accurate monitoring of corneal ablation processes.

2. Experimental setup and procedure

2.1. Ablation procedure

Laser ablation was carried out at the Laser Micro-processing Facility of the Universidad de Salamanca. A Ti:sapphire oscillator (Tsunami, Spectra Physics, Inc., Mountain View, CA) and a regenerative amplifier system (Spitfire, Spectra Physics, Inc., Mountain View, CA) based on chirped pulse amplification (CPA) technique were used to ablate the corneal tissue. The laser system delivered 120 fs linearly polarized pulses at a repetition rate of 1 kHz and a central wavelength of 795 nm. The maximum available pulse energy was 1.1 mJ. A half-wave plate and a linear polarizer, together with a set of neutral density filters were used to set the

#150262 - $15.00 USD Received 1 Jul 2011; revised 27 Sep 2011; accepted 27 Sep 2011; published 3 Oct 2011

required pulse energy. The transverse mode of the laser beam was nearly Gaussian with a radius of 4.5 mm (measured at $1/e^2$ in intensity).

A 20x microscope objective lens (NA = 0.40) focused the beam, as a trade-off between a long-working distance to safely operate with no risk of contact with the sample (chicken cornea, see below), and a large numerical aperture to avoid ablation at the surface during the irradiation. The micro-processing was carried out in air.

The chicken head was placed and attached to a computer controlled XYZ stage. The eye under analysis was facing up towards the microscope objective. An auxiliary laser (633 nm) passing through the objective helped us to find the apex of the cornea by centering the beam reflection with the direction of incidence. Afterwards the (attenuated) fs laser beam was focused on the corneal apex and then the XYZ stage was moved a pre-established distance ("focusing parameter") towards the objective, to set the plane of irradiation within the corneal tissue.

The laser beam followed a spiral covering a circular area of 1 mm in diameter and two different photo-disruptive patterns were induced inside the chicken cornea. In one case, the sample was irradiated at equally spaced points of the spiral (ablation pattern #1). The irradiation was controlled by a mechanical shutter that was opened during 100 ms at each point (i.e. 100 shots). The pulse energy was 6 μJ (measured after the focusing lens). The separation between consecutive points and the pitch were set to 15 μm. For the second pattern the laser was continuously irradiating the sample with scanning speed of 2 mm/s, a pitch of 25 μm, and energy of 1.7 μJ per pulse (ablation pattern #2).

2.2. Sample preparation

Eyes of adult chickens with similar age were used in this work. The chicken heads were moved in low temperature conditions from the abattoir to the ablation lab, and processed within two hours after death. To avoid corneal dehydration during the ablation procedure, drops of BBS were instilled every few seconds. Immediately after the fs laser photodisruption the eyes were enucleated and the corneas excised with a trephine. Specimens were immersed in a culture medium consisting of L-15 medium (Leibovitz) and L-glutamine and moved to the multiphoton imaging lab in an appropriate container to be imaged a few hours later.

Immediately after multiphoton imaging the corneas were fixed with buffered formalin 10% and moved to the histology lab. Then, they were washed in buffer phosphate 0.1 M and embedded in paraffin wax. Five micron sections were stained with Hematoxylin–Eosin (H&E). The sections were examined and photographed with a Zeiss Axiophot microscope (Zeiss, Oberkochen, Germany).

2.3. Backscattering-mode adaptive-optics multiphoton microscope

Multiphoton (nonlinear) microscopy was performed at the Laboratorio de Óptica of the Universidad de Murcia. The instrument has been described previously [29,30]. Briefly, the system combines a mode-locked Ti:sapphire laser (Coherent, St. Clara, CA; 110 fs pulses, 76 MHz repetition rate) and a modified inverted microscope (TE2000-U, Nikon, Corp., Tokio, Japan). An adaptive optics (AO) module composed of a real-time Hartmann-Shack wavefront sensor and a deformable mirror [30,31] was used to compensate for the laser beam aberrations in closed-loop. A pair of non-resonant galvanometric mirrors allowed the XY scanning and a DC-motor controlled the location of the focus position along the Z axis. The nonlinear signals generated at the sample (both TPEF and SHG) were collected through the same objective (backscattering configuration) as in the illumination pathway (20x, NA = 0.5), passed a dichroic mirror which separated the excitation from the emission wavelengths and reached the photomultiplier tube (connected to a photon-counting unit). A long-pass and a narrow-band filter were inserted in front of the detector to isolate the TPEF and SHG signals respectively. All the system was computer-controlled by custom LabView™ software. Image processing was performed with both MatLab™ and ImageJ. The average illumination power never exceeded 150 mW at the plane of the specimen and the wavelength used was 760 nm. Taking into account the technical details of the laser and the actual experimental conditions, the XY

#150262 - $15.00 USD Received 1 Jul 2011; revised 27 Sep 2011; accepted 27 Sep 2011; published 3 Oct 2011

scanning speed here used is about two orders of magnitude below the values reported to produce changes in the tissue [32]. This ensures that the samples do not suffer additional changes during imaging.

3. Results

3.1. Nonlinear microscopy imaging of the intact chicken cornea

Nonlinear images of the intact *ex vivo* chicken cornea were firstly acquired. Both the epithelium and the entire corneal stroma were imaged. The set of corneas here examined presented a total thickness of about 250 µm (including the epithelial layers).

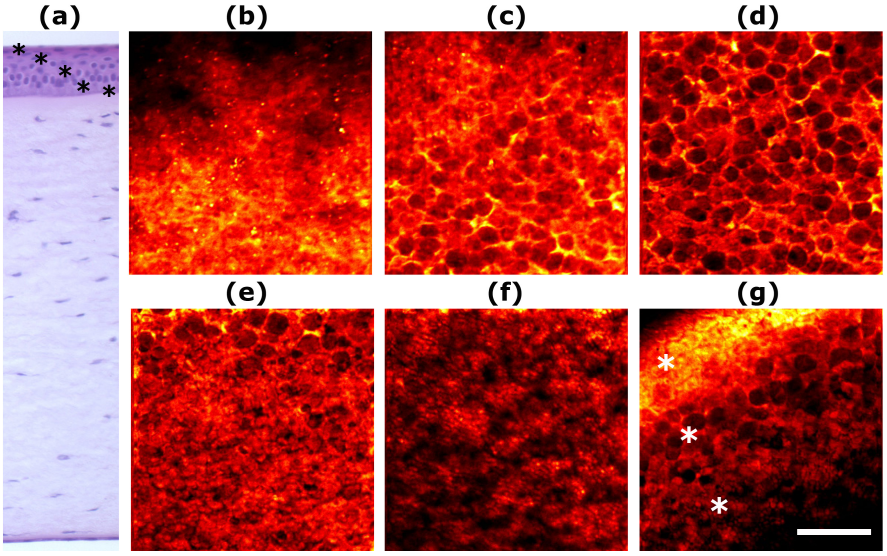

Fig. 1. (a) Transversal histological section of a chicken cornea. (b)-(f) TPEF images of the different layers within the epithelium: superficial cells (b), wing cells (c-d), basal cells (e-f). The three types of epithelial cells can be observed together in (g) (see stars). Bar length: 50 µm.

The corneal epithelium (for the central cornea) was imaged through TPEF microscopy. This is composed of several layers of different cells, in which superficial, wing and basal cells are lined up from surface to bottom with increasing nucleus-to-cytoplasm ratio as depth increases, except basal cells that appear like small disks [33,34]. Figures 1(b-f) show a set of TPEF images of the epithelium separated 10-µm in depth. A conventional transversal histological section of the chicken cornea is also shown for comparison (Fig. 1(a)). The corresponding imaged layers within the epithelium are labeled with stars in Fig. 1(a). It can be observed that for every layer the TPEF signal is originated from the cell cytoplasm, while the nucleus and the cell boundary remain dark. Superficial cells are depicted in Fig. 1(b) while wing cells can be observed in Fig. 1(c-d). The basal cells are illustrated in Fig. 1(f). Figure 1(e) presents the interface between wing and basal cells. Finally in Fig. 1(g) the three different epithelial cell layers are imaged together (see stars), making visible their morphological differences. This image was obtained in a peripheral area of the chicken cornea where the corneal surface is not perpendicular to the microscope optical axis.

Making use of the SHG signal, the stroma morphology was also explored. The corneal stroma was found to be about 200-µm thick. Figure 2 shows a series of SHG images of the chicken stroma at different depths spaced ~30 µm. A visual examination shows collagen lamellae lying mostly parallel to the corneal surface. For every depth position, long collagen bundles run parallel to each other with some orthogonal interweaving. For every Z-position this pattern systematically rotates and a gradual angular shift of the layers is observed.

#150262 - $15.00 USD Received 1 Jul 2011; revised 27 Sep 2011; accepted 27 Sep 2011; published 3 Oct 2011

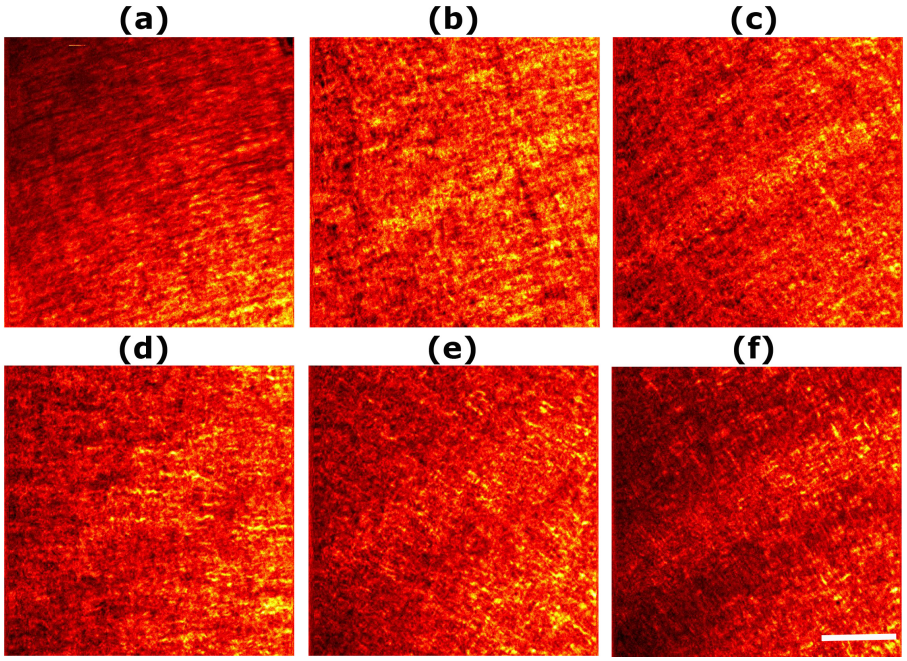

Fig. 2. SHG signal from the collagen of the chicken corneal stroma at different depths (spaced ~30 μm). Bar length: 50 μm.

3.2. Histological sections of ablated corneas

As explained in Section 2.2, the corneas were fixed immediately after multiphoton imaging and analyzed with a bright-field (linear) microscope. Despite this histological analysis was the last step in our experiment, it is worth to show how the ablation patterns look like before presenting the multiphoton results.

Figure 3 presents the histological sections where the two different ablation patterns are seen. Both the cavities and the continuous line according to the framework described above can be seen. Moreover, despite the manipulation of the corneal tissue during ablation and multiphoton imaging, the epithelial layer is still observed under regular microscopy.

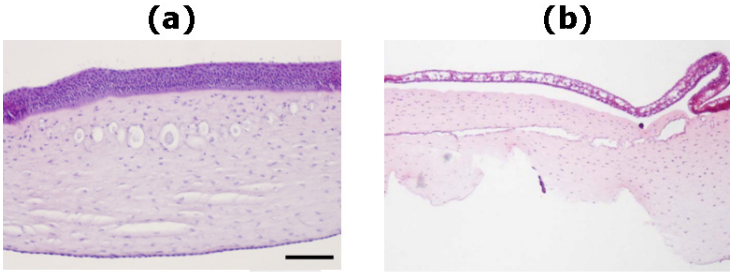

Fig. 3. Histological sections of chicken corneas showing the intrastromal ablation patterns #1 (a) and #2 (b). Bar length: 200 μm.

3.3. Nonlinear microscopy of the intrastromal ablation patterns

With the assistance of AO nonlinear microscopy, the targeted region of intrastromal ablation was also determined and analyzed. Figure 4 presents the results for the two different ablation patterns: spaced individual points (pattern #1, upper panels) and continuous line (pattern #2, bottom row).

#150262 - $15.00 USD Received 1 Jul 2011; revised 27 Sep 2011; accepted 27 Sep 2011; published 3 Oct 2011

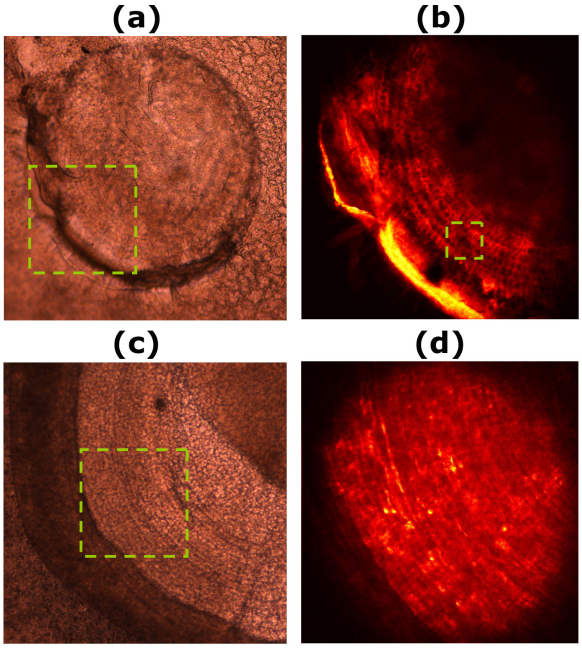

Fig. 4. Microscopy imaging illustrating the intrastromal laser surgery: bright-field (a, c) and nonlinear images (b, d). Upper and bottom rows correspond to ablation patterns #1 and #2 respectively. Each square sets the size of the adjacent image. The size of images (b) and (d) is 840x840 μm^2.

For each specimen, bright-field microscopy images were firstly acquired (Figs. 4(a) and 4(c)). This allows a better location of the area to be imaged with the nonlinear technique (see dashed green squares). Due to the corneal curvature it can be seen how ablation patterns affect the corneal surface at the more peripheral region. The external structure of the spiral-shaped ablation profile is observed. However both the edges of the laser cuts and the cavities within the stroma cannot be observed with this microscopy mode. On the opposite, the ablation patterns can easily be identified at a certain depth in the nonlinear (SHG) microscopy images. In particular Fig. 4(b) presents the image corresponding to a depth of 140 µm from the outer epithelium layer while Fig. 4(d) was recorded at 180 µm.

Three-dimensional reconstructions were also performed from stacks of SHG images. These helped in the monitoring and visualization of the intrastromal ablation pattern. An example of a 40-µm thick stromal area around the ablation zone (pattern #1) is shown in Fig. 5.

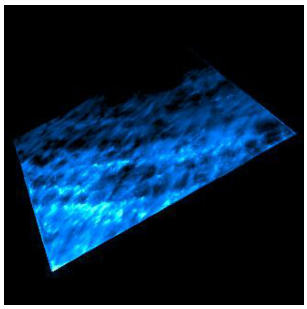

Fig. 5. 3D representation of the intrastromal ablated area. 20 individual SHG images of planes 2-µm apart were used for the reconstruction. Blue color has been used for a better visualization of the cavities of pattern #1. Image size corresponds to the square inset in Fig. 3(b).

#150262 - $15.00 USD Received 1 Jul 2011; revised 27 Sep 2011; accepted 27 Sep 2011; published 3 Oct 2011

From the stacks of SHG images along the entire corneal depth, additional volume renderings can also be reconstructed. Figure 6 shows these volume renderings for both ablation patterns.

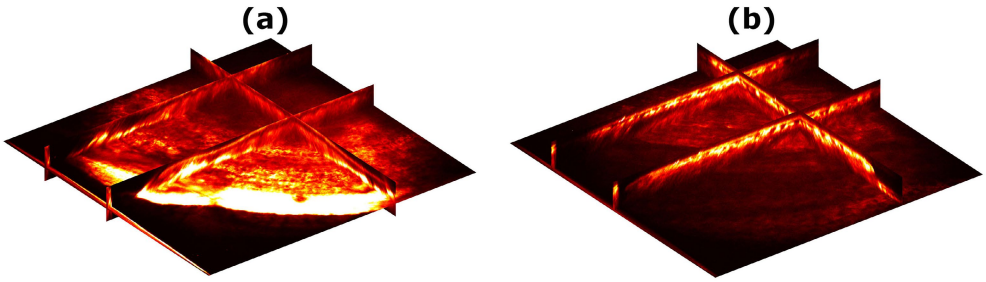

Fig. 6. 3D (nonlinear microscopy) images of chicken corneas showing the two different ablation patterns: (a) #1 and (b) #2.

An analysis of the ablated corneas as a function of depth was also performed using nonlinear imaging microscopy. Starting from the epithelium, Fig. 7 presents (for ablation pattern #1) a set of images with increasing depth and a spacing of 40 μm between planes. The imaged region corresponds to the square area in Fig. 4(a) which was not perpendicular to the microscope optical axis. Figures 7(a-c) depict the nonlinear signal originated from the different cells of the epithelium. It can be observed how the epithelium presents some folded regions ("wrinkles") as a side effect of the ablation procedure at the more peripheral corneal area. To avoid this, the depth of the ablation profile must be corrected as we leave the centre of the spiral to compensate for the corneal curvature. In Fig. 7(d), at a depth of about 120 μm the more peripheral part of the ablation pattern #1 starts to appear. When imaging deeper, more areas of this intrastromal pattern are clearly observed (Figs. 7(e-f)). For deeper stromal regions the ablation pattern disappears (Figs. 7(g-h)). All this can be better observed in the movie of Fig. 8.

Corneas with ablation pattern #2 were also imaged for similar experimental conditions. Results are depicted in Fig. 9. While the different epithelial cells are imaged in Figs. 9(a-e), the ablation pattern is visible at about 150 μm (area at the bottom) together with part of

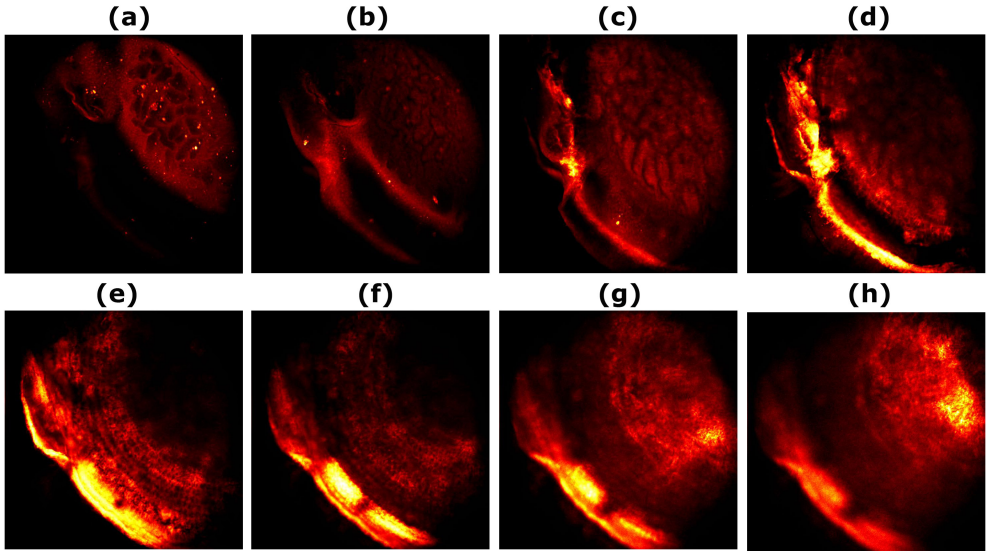

Fig. 7. Nonlinear microscopy images of an ablated chicken cornea (pattern #1) at different depths (spaced 40 μm). The imaged area was 840x840 μm^2.

#150262 - $15.00 USD Received 1 Jul 2011; revised 27 Sep 2011; accepted 27 Sep 2011; published 3 Oct 2011

epithelium of the folded area above mentioned (Figs. 9(f-g)). Finally Fig. 9(h) clearly depicts a large area of the intrastromal ablation pattern. Similar to pattern #1, the spiral pitch for pattern #2 was also measured at different locations.

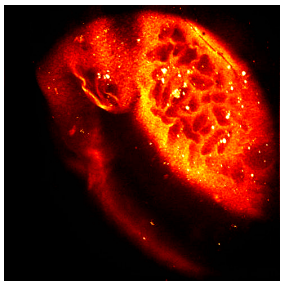

Fig. 8. (Media 1) Movie showing the stack of nonlinear images at different depths in an ablated cornea.

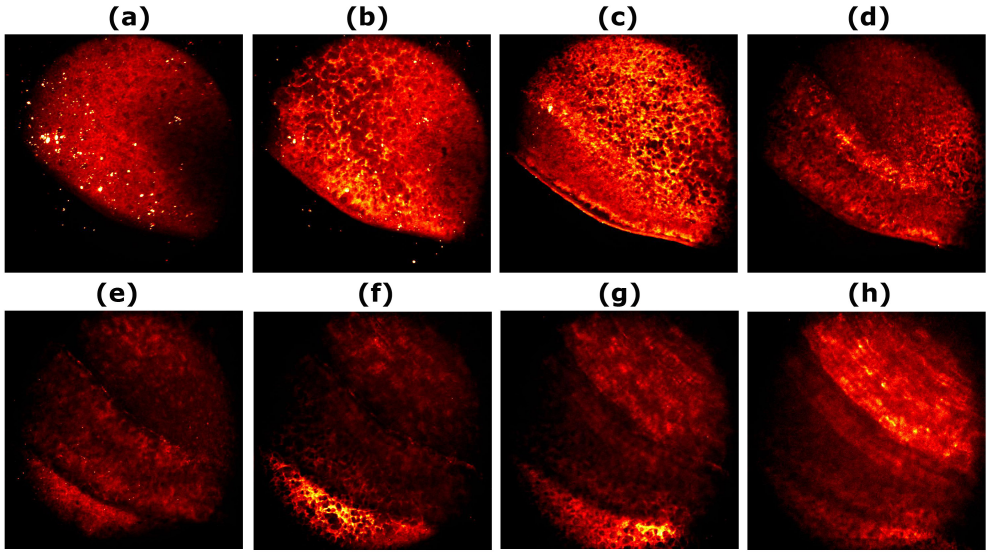

Fig. 9. Nonlinear microscopy images of an ablated chicken cornea (pattern #2) corresponding to planes 30 μm apart. Image dimensions are the same as for Fig. 6.

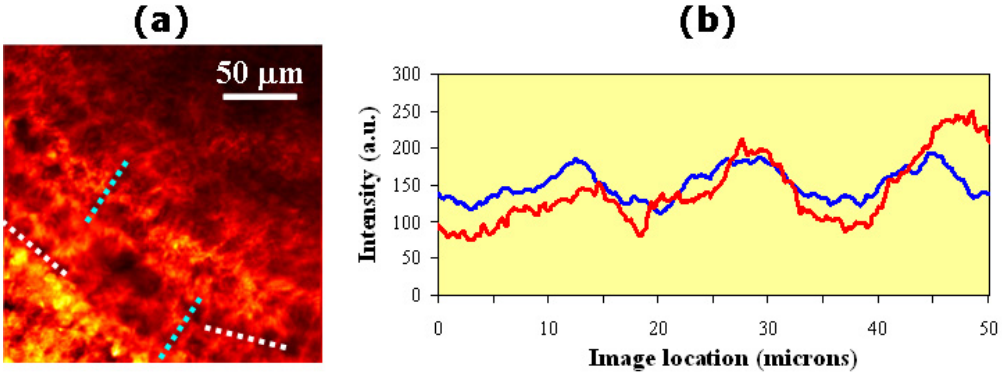

Fig. 10. (a) Examples of locations across the nonlinear microscopy image of an ablated chicken cornea (pattern #1) where the intensity profile was computed. (b) Intensity along two different sections crossing the location of three cavities of the intrastromal pattern.

#150262 - $15.00 USD Received 1 Jul 2011; revised 27 Sep 2011; accepted 27 Sep 2011; published 3 Oct 2011

Once the intrastromal pattern #1 was visualized, the performance of the ablation procedure was evaluated by measuring the distance between pairs of consecutive cavities. This distance was quantified by computing the intensity reflectance across different locations of the image as shown by means of dotted white lines in Fig. 10(a). As an example Fig. 10(b) plots the image intensity along two different lines. In particular, the inter-cavity distance was measured for a number of adjacent cavities at different locations across the ablation pattern. The average distance was 14 ± 2 μm, what agrees well with the nominal value of 15 μm described in Section 2. Using a similar procedure (see dotted blue lines in Fig. 10(a)), the pitch of the spiral was also computed at different locations, resulting an average value of 17 ± 3 μm (nominal value = 15 μm).

For pattern #2, a similar procedure was used. However since this ablation pattern was continuous, only the pitch of the spiral was measured at different locations. The mean value was 19 ± 2 μm that lies below the nominal value of 25 μm.

4. Discussion

A combined use of corneal ablation procedures and backscattering AO multiphoton microscopy using NIR fs pulses has been demonstrated. Intrastromal patterns can be monitored and tested in *ex vivo* corneas without the need of fixation or staining. Corneal ablation causes structural changes within the cornea in a controlled manner. Both epithelial cells and the corneal stroma morphology are visualized.

The high photon flux of these ultrafast pulsed light sources, together with a "reduced" mean power, allowed exploring the nonlinear interaction between light and matter. Ultrashort laser disruption of cells or tissues has become an effective technique with very innovative experimental applications [9]. In particular, these laser systems make multiphoton imaging and micro-processing mechanisms effective when applied to corneal tissues [16,17,27,28]. The NIR light provided by these sources is convenient due to the transparency of the human eye at this spectral range, increasing the penetration depth for both imaging and ablation.

A number of works have reported different photodisruption patterns produced within the corneal stroma. Their evaluation has often been carried out by means of histological sections [10,22,26,35] and confocal microscopy [36], but multiphoton imaging has not been used very often.

Han and colleagues reported individual cavitation bubbles and corneal cuttings induced in porcine corneas (Nd:glass laser, λ = 1.06 μm). These corneas were successfully imaged through nonlinear microscopy in transmission mode. They used a wavelength of 880 nm and an oil immersion objective (NA = 1.4) for signal collection [27]. Wang and associates [28] also visualized intrastromal cuts (Ti:sapphire laser, λ = 800 μm) in *ex vivo* rabbit corneas. Although their microscope worked in backscattered mode, a high numerical aperture (1.3, oil) objective was used. In rabbit corneas, Morishige and co-authors reported some preliminary results on both backward and forward SHG images of corneal collagen following photodisruption produced by a commercial surgical laser [36].

Unlike previous works using water or oil immersion objectives with larger NAs, our multiphoton microscope uses a non-immersion objective in a backscattered mode. Others have reported that this configuration provides weak nonlinear signals from corneas tissues [37], however our setup provides us with high-quality images of the different corneal layers (see also [38] for further information). The effectiveness of our microscope was mainly based on the optimization/correction of aberrations, combined with a backscattering configuration. This experimental configuration has been proven to provide high quality nonlinear images (both TPEF and SHG) [29–31,38,39].

The ablation process is highly nonlinear and intensity dependent. Then, the affected area is reduced to a tiny region around the focal volume, what allows generating arbitrary geometries with improved accuracy and smoothness. When the analysis of the tissue effects is done through histological slices, artifacts in the size and the shape of the cavities of the ablation might appear as a result of the excessive manipulation of the samples [26]. Alternatively,

#150262 - $15.00 USD Received 1 Jul 2011; revised 27 Sep 2011; accepted 27 Sep 2011; published 3 Oct 2011

nonlinear microscopy offers an efficient tool to analyze the morphology of the corneal stroma in a minimally invasive manner [27,36–39].

When visualizing the ablated corneal stroma, a decrease in the nonlinear signal of the areas where the ablation took place was observed. This loss of signal is a result of the disruption of the non-centrosymmetric structure of the collagen fibers within the stroma which is the structure associated with SHG signals. This was also shown in the work by Han and colleagues although they did no pay much attention to this "absence of signal" [16,27]. Alternatively, other authors observed a strong increase of the nonlinear autofluorescence intensity (TPEF) of the ablated area in corneas [17,28,40] and in other type I collagen tissues [40,41]. This was related to the formation of new autofluorescent substances during the surgery process (such as tyrosine dimers). However this effect was not explored in depth either.

The clinical use of fs lasers in refractive surgery is basically restricted to corneal flap cutting [13]. Ablation procedures are still performed by excimer laser systems [6–8]. The flap creation is performed by fs lasers with low repetition rate (in the range from Hz to kHz) by inducing photodisruption and destructive optical breakdown in the more external corneal tissue. The use of fs lasers in conductive keratoplasty has also a great potential in clinical environments [21,22,42]. The main advantage originates from the feasibility for precise cutting of any arbitrary geometry (zig-zag, top hat patterns,…) on both the donor and the recipient eye, increasing resistance and accelerating the healing process.

However recent techniques such as fs lentotomy [23] and intratissue refractive index shaping (IRIS) [24] have introduced new insights into research fields such as visual optics and ocular surgery. The former proposes a treatment for presbyopia (loss of flexibility in the crystalline lens with age) through the formation of small cuts inside the lens capsule by fs pulse photodisruption to recover flexibility. The latter creates periodic gratings in the corneal stroma or the cortex of the lens to change the refractive index. This technique may represent an alternative method to classical refractive surgery.

Based on the results reported here, the replacement of excimer laser systems by NIR fs lasers would be of high interest. This might be based on the fact that NIR light propagates with negligible absorption through the tissue. NIR fs ablation procedure (at a higher repetition frequency) provides precise intratissue processing without collateral damage such as mechanical or optical destruction of the epithelial layer.

Although actual experiments used *ex vivo* corneas, the results found are indispensable to establish background knowledge, prior to an *in vivo* examination approach. To our knowledge only preliminary studies have reported NIR ablation [35,36,43] and multiphoton microscopy in living eyes of animal models [35,43,44]. Future *in vivo* applications would be helpful in exploring the collagen reorganization, regeneration, healing processes and disease progression.

To conclude, NIR fs laser technology has been used to perform intrastromal surgery in *ex vivo* chicken corneas and to image the ablated tissue through multiphoton microscopy. Corneal NIR ablation has been proven to be precise, with minimized thermal effects and surrounded regions hardly affected. The surgical performance has been visualized and precisely evaluated in a non-invasive manner without the use of staining procedures. Although in this work surgical and imaging investigations were conducted sequentially, a further combination of both surgical and monitoring functions into a single fs laser system has the potential to be an attractive tool. Potential *in vivo* implementations based on the combination of both techniques (ablation plus imaging) would be of special interest in vision research and future clinical environments, mainly for high-resolution imaging of ocular tissues, diagnosis and NIR corneal surgery monitoring.

Acknowledgments

This work has been supported by "Ministerio de Educación y Ciencia," Spain (grant nos. FIS2007-64765, FIS2010-15746 and Consolider Program SAUUL CSD2007-00013) and "Fundación Séneca," Murcia, Spain (grant 04524/GERM/06).